Published OnlineFirst May 21, 2019; DOI: 10.1158/2326-6066.CIR-18-0881

Research Article

Cancer Immunology Research

An Artificial Antigen-Presenting Cell Delivering 11 Immune Molecules Expands Tumor Antigen–Specific CTLs in *Ex Vivo* and *In Vivo* Murine Melanoma Models

Lei Zhang, Shilong Song, Xiaoxiao Jin, Xin Wan, Khawar Ali Shahzad, Weiya Pei, Chen Zhao, and Chuanlai Shen

Abstract

Antigen-presenting cells expand antigen-specific T cells *ex vivo* and *in vivo* for tumor immunotherapy, but are time-consuming to generate and, as live cells, raise biosafety concerns. An alternative is found in cell-free artificial antigen-presenting cells (aAPC), but these only present two or three kinds of immune molecules. Here, we describe a multipotent artificial antigen-presenting cell (MaAPC) that delivered 11 kinds of immune moleclues. This MaAPC simulated natural APCs through the concurent coupling of target antigens (H-2K^b/TRP2$_{180–188}$-Ig dimers and H-2D^b/gp100$_{25–33}$-Ig dimers), costimulatory molecules (anti-CD28, anti–4-1BB, and anti-CD2), and "self-marker" CD47-Fc onto surface-modified polylactic-co-glycolic acid microparticles (PLGA-MP). These PLGA-MPs also encapsulated cytokines (IL2 and IL15), a chemokine (CCL21), and checkpoint inhibitors (anti–CTLA-4 and anti–PD-1). Culture of MaAPCs with naïve T cells for 1 week elevated the frequencies of TRP2$_{180–188}$–specific and gp100$_{25–33}$–specific CTLs to 51.0% and 43.3%, respectively, with enhanced cytotoxicity. Three infusions of MaAPCs inhibited subcutaneous melanoma growth in a mouse model and expanded TRP2$_{180–188}$ and gp100$_{25–33}$–specific CTLs 59–86-fold in peripheral blood, 76–77-fold in spleen, and 205–212-fold in tumor tissue, in an antigen-specific manner. Compared with conventional aAPCs carrying two or three immune molecules, the 11-signal MaAPCs exerted greater impact on T cells, including activation, proliferation, cytotoxicity, differentiation to memory CTLs or regulatory T cells and cytokines profiles, without detected side effects. Such MaAPCs could be used to individualize tumor immunotherapy.

Introduction

On-target expansion of antigen-specific T cells is one strategy for tumor immunotherapy (1–3). Antigen-presenting cells (APC), especially dendritic cells (DC), can facilitate immune responses, but are time-consuming and costly to generate, can stimulate nonspecifically, and are subject to biosafety concerns (4, 5). Therefore attention has shifted toward artificial APCs (aAPC), which have been developed to induce therapeutic cellular immunity (6–8) on both cell-based (9–11) and polymer technologies (8, 12–14). Polymer aAPCs can be generated by cocoupling antigenic peptide-loaded major histocompatability complexes (pMHC, first signal) and anti-CD28 (second signal) onto micro- or nanoscale magnetic beads or polyester latex beads (13–18). Polymer aAPCs are more amenable to rapid and large-scale manufacturing with uniform quality than cellular aAPCs, and raise fewer biosafety concerns than do live cells. However, most polymeric aAPC fabrications use two or three kinds of molecules on rigid beads, e.g., magnetic or latex beads. Few studies use multiple first signals, second signals, and third signals as well as a biodegradable scaffold suitable for *in vivo* use.

With an eye toward clinical applications, we developed a biodegradable and multipotent aAPC system carrying 11 kinds of immune molecules. Polylactic-co-glycolic acid (PLGA) is a biocompatible, biodegradable, and notoxic polymer used in drug and vaccine delivery systems in humans (19–21). Here, cell-sized PLGA microparticles (PLGA-MP) were generated and polyethylenimine-modified as a scaffold to cocouple the tartget antigens (H-2K^b/TRP2$_{180–188}$–Ig dimers, H-2D^b/gp100$_{25–33}$–Ig dimers), costimulatory molecules (anti-CD28, anti–4-1BB, anti-CD2), and "self-marker" CD47-Fc on their surface, and to co-encapsulate cytokine (IL2, IL15), chemokine (CCL21), and checkpoint inhibitors (anti–CTLA-4, anti–PD-1). Phenotypes and corelease efficiency were analyzed, and the synergistic effects on expanding tumor antigen–specific CTLs were evaluated *ex vivo*. The multipotent aAPCs (MaAPC) were intravenously administered into a melanoma mouse model. We then investigated therapeutic outcomes, tissue distribution, mechanism, and side effects. I*n vivo* effects of MaAPCs were compared with control MPs carrying 9, 8, 6, 5, or 2 kinds of immune molecules.

Department of Microbiology and Immunology, Medical School, Southeast University, Nanjing, China.

Note: Supplementary data for this article are available at Cancer Immunology Research Online (http://cancerimmunolres.aacrjournals.org/).

Corresponding Author: Chuanlai Shen, Southeast University Medical School, 87 Dingjiaqiao Rd, Nanjing, Jiangsu Province 210009, China. Phone: 86-25-83272454; Fax: 86-25-83324887; E-mail: chuanlaishen@seu.edu.cn

Cancer Immunol Res 2019;7:1188–201

doi: 10.1158/2326-6066.CIR-18-0881

Published OnlineFirst May 21, 2019; DOI: 10.1158/2326-6066.CIR-18-0881

Materials and Methods

Mice and cell lines

C57BL/6J female mice were from the Comparative Medicine Center of Yangzhou University (Yangzhou, China), maintained in the specific pathogen-free Laboratory Animal Centre of Southeast University (Nanjing, China), and were used in experiments at 8 to 12 weeks of age. Animal welfare and experimental procedures were approved by the Animal Ethics Committee of Southeast University and performed in accordance with the Guidelines for the Care and Use of Laboratory Animals (Ministry of Science and Technology of China, 2006) and the National Institutes of Health Guide for the Care and Use of Laboratory Animals (NIH Publications No. 8023, revised 1978). All mouse cell lines including melanoma B16F10, fibrosarcoma S180, myeloma SP2/0, and lymphoma Yac-1 were from the Cell Bank of Type Culture Collection of Chinese Academy of Sciences in 2017, and tested for *Mycoplasma* by Hoechst staining before use. In general, the cell lines were cultured for 2 weeks during our experiments, but were not authenticated in the past year.

Fabrication of PLGA-MPs with encapsulated cytokines, chemokines, and antibodies

PLGA-MPs were fabricated using a double-emulsion water-in-oil-in-water (W1/O/W2) method as described (22), with modifications: 100 mg of PLGA (Daigang Company) was initially dissolved in 5 mL dichloromethane (oil phase, O) and followed by the addition of 200 μL 0.1 mol/L PBS (for Blank-MPs) or the 200 μL aqueous solution containing 2.5 μg of IL2, 2.5 μg of IL15, 5 μg of CCL21 (PeproTech), 12.5 mg of anti–PD-1, and 12.5 mg of anti–CTLA-4 (Bio X Cell) as internal water phase (W1). The W1/O emulsion was formed by sonicating the mixture for 30 seconds under 20 kHz and 30% amplitude using a probe sonicator (Sonics and Materials). The primary W1/O emulsion was quickly mixed with 5 mL of 4% (w/v) PVA solution (external water phase, W2) and homogenized (T-18 digital ULTRA-TURRAX IKA, Germany) for 30 minutes at 6,000 rpm. Then, 5 mL of deionized water was added and the solution was stirred overnight at room temperature to evaporating dichloromethane. The final solution was centrifuged at 3,000 rpm for 5 minutes to collect microparticles (MP). The harvested MPs were washed to remove PVA. The MPs were activated using EDC and NHS and then added dropwise into the polyethylenimine (PEI; Sigma-Aldrich) solution with magnetic stirring and incubated for another 2 hours at 20°C. Finally, PEI-conjugated MPs were washed twice to remove the free PEI with deionized water and stored at 4°C for use. The consequent PLGA-MPs encapsulating IL2, IL15, CCL21, anti–PD-1, and anti–CTLA-4 were termed MP_{5+}. In parallel, the control PLGA-MPs were also generated using similar methods, such as Blank-MPs (without encapsulation), MP_{2+} (encapsulated with IL2 and IL15), and MP_{3+} (encapsulated with IL2, IL15, and CCL21).

Characterization of PLGA-MPs

The resulting PLGA-MPs were characterized for morphology using scanning electron microscopy (SEM, ZEISS EVO 18). The size distribution was measured by a laser diffraction particle size analyzer (Mastersizer 3000, Malvern Instruments), and the ζ potential of MPs was measured using a Zeta PALS instrument (Brookhaven Instruments Corporation).

The encapsulation efficiency and sustained release of PLGA-MPs were determined as described (22). To determine the amount of IL2, IL15, CCL21, anti–PD-1, and anti–CTLA-4 encapsulated into PLGA-MPs, 1×10^7 PLGA-MPs were resuspended in 1 mL of 0.1 mol/L NaOH/0.5% SDS solution. After 24-hour incubation at 37°C on a shaker, the suspension was centrifuged for 5 minutes at 3,000 rpm. The supernatant was collected and followed by the quantitative detection of IL2, IL15, CCL21, anti–PD-1, and anti–CTLA-4 using ELISA kits (eBiosciences) according to the manufacturer's protocols. In order to monitor the dynamic release of these molecules from the PLGA-MPs, 1×10^7 PLGA-MPs were resuspended in 1 mL of sterile 0.1 mol/L PBS and incubated with rotation on a rotator (200 rpm) at 37°C. At the indicated time points, the supernatant was collected after centrifugation and an equal volume of fresh medium was supplemented. The amount of IL2, IL15, CCL21, anti–PD-1, and anti–CTLA-4 in the supernatant was quantified using the ELISA kits as described.

Preparation and phenotype analyses of MaAPCs

The PEI-conjugated MP_{5+} (1×10^8) were coincubated with H-$2K^b$/$TRP2_{180–188}$–Ig dimers (5 μg), H-$2D^b$/$gp100_{25–33}$–Ig dimers (5 μg; BD Biosciences), anti-CD28 (10 μg), anti-4-1BB (10 μg), anti-CD2 (10 μg), and CD47-Fc (1 μg) (R&D Systems) in sterile 0.1 mol/L PBS at 4°C for 24 hours on a rotator. The resulting MPs were incubated in blocking buffer (0.1 mol/L PBS containing 10% BSA) at 4°C for another 24 hours with rotation. Finally, the suspension was centrifuged and particles were harvested. After washing with PBS, the resultant aAPCs, termed MaAPCs, were resuspended in sterile PBS, stored at 4°C and used within 24 hours. In parallel, several control MPs were generated in a similar manner: MP^{2+} (H-$2K^b$/TRP2-Ig and H-$2D^b$/gp100-Ig onto MPs), MP^{5+} (H-$2K^b$/TRP2-Ig, H-$2D^b$/gp100-Ig, anti-CD28, anti-4-1BB and anti-CD2 onto MPs), MP^{6+} (H-$2K^b$/TRP2-Ig, H-$2D^b$/gp100-Ig, anti-CD28, anti-4-1BB, anti-CD2 and CD47-Fc onto MPs); MP^{6+}_{2+} (six indicated molecules onto MPs with IL2 and IL15 inside MPs), MP^{6+}_{3+} (six indicated molecules onto MPs with IL2, IL15, and CCL21 inside MPs).

In order to analyze the phenotypes of MaAPCs, 1×10^7 MaAPCs were stained, respectively, with PE-anti-mouse H-$2K^b$, PE-anti-mouse H-$2D^b$, FITC-anti-hamster IgG (binds to anti-CD28), FITC-anti-rat IgG (binds to anti-CD2), PE-anti-goat IgG (H + L; binds to anti-4-1BB), APC-anti-human IgG1 Fc (binds to CD47-Fc; 1 μg for each antibody, R&D Systems) for 30 minutes at 4°C in the dark. After washing, for each sample, 2×10^5 particles were acquired on a FACSCalibur flow cytometer (BD Biosciences) and analyzed with FlowJo software (Tree Star). The sustained release of IL2, IL15, CCL21, anti–PD-1, and anti–CTLA-4 was detected as described.

Ex vivo expansion of TRP2- and gp100-specific $CD8^+$ T cells by MaAPCs

Splenocytes were harvested from naïve B6 mice (H-2^b), and lymphocytes were enriched by density gradient centrifugation. The spleen lymphocytes (SPC; 10^5 cells per well) were cocultured with blank PLGA-MPs (blocked with BSA), MP_{5+}, MP^{6+}, or MaAPCs (10^5 beads per well) in 96-well round-bottom plate and maintained in RPMI-1640 medium supplemented with 10% FBS in the absence of IL2 (50 U/mL of IL2 was added in Blank-MPs group) for 7 days. Then, cocultures were harvested to detect the frequency of $TRP2_{180–188}$ and $gp100_{25–33}$-specific $CD8^+$ T cells by pMHC multimer staining. Briefly, cells were incubated with anti-mouse CD16/CD32 for 30 minutes at 4°C to block Fc

Published OnlineFirst May 21, 2019; DOI: 10.1158/2326-6066.CIR-18-0881

receptors, then incubated with a mixture of H-2K^b/TRP2-Ig (or H-2K^b/gp100-Ig) dimers and APC-anti-mouse IgG1 (BD Biosciences) for 1 hour at 4°C in the dark. After washing, FITC-anti-mouse CD8 and PE-anti-mouse CD3 (eBiosciences) were added for an additional 30 minutes at 4°C and followed by flow cytometry.

Cytotoxicity assay of CTLs

After 1-week incubation with MaAPCs, SPCs were harvested for use as effector cells. The mouse melanoma cell line B16 (H-2^{b+}/TRP2$^+$), fibrosarcoma cell line S180 (H-2^{b+}/TRP2$^-$), and myeloma cell line SP2/0 (H-2^{b-}/TRP2$^-$) were used, respectively, as target cells (1×10^4 cells per well). The 4-hour cytotoxicity assay was then performed as previously described (18). Mouse Yac-1 cells (5×10^4 cells/well) were added to prevent cytolysis of target cells by the NK cells present in the splenocyte population. SPCs and Yac-1 cells were prestained with 10 μmol/L CFSE (BD Pharmingen) for 20 minutes at 37°C and immediately washed three times with ice-cold RPMI-1640 medium. The CFSE-labeled effector cells and Yac-1 cells were then seeded in round-bottom 96-well plates (BD Falcon) and coincubated with target cells in RPMI-1640 medium with 10% FBS at 37°C in a 5% CO_2 atmosphere for 4 hours. The cells were seeded at varying ratios of effector-to-target cell numbers. Cells were then collected, resuspended in 1% BSA/PBS, and acquired on a FACSCalibur (BD Biosciences) after staining with 7-AAD. CTL activity was calculated as the percentage of 7-AAD$^+$ cells within the CFSE$^-$ cell population.

In vivo expansion of antigen-specific CD8$^+$ T cells and tumor inhibition by MaAPCs infusion

On day 0, B6 mice were injected subcutaneously (s.c.) in the right flank with B16 cells (or S180 cells) at a dose of 1×10^6 cells per mouse. Mice were then randomized into 7 groups and infused via tail vein with MaAPCs, MP^{6+}_{3+}, MP^{6+}_{2+}, MP^{6+}, MP^{5+}, MP^{2+}, or Blank-MPs on days 7, 9, and 11 (1×10^7 MPs per mouse per time point). On days 7 (before treatment) and 28 (after treatment), peripheral blood was collected from the orbital veins. Spleens and tumors were also collected on day 28 from each mouse. Peripheral blood mononuclear cells (PBMC) and SPCs were then prepared routinely. Single-cell suspensions derived from tumor tissues were prepared as described (23). Briefly, tumor tissues minced into small pieces were digested with collagenase type VIII (1.5 mg/mL; Sigma) for 2 hours at 37°C with gentle agitation. Consequently, tissues were passed through 70-mm nylon mesh filters (BD Biosciences) and transferred to DMEM High Glucose media supplemented with 2% FCS. After centrifugation (1,000 × *g*, 10 minutes), pellets were resuspended in 2% FCS-PBS. Then, the frequency of $TRP2_{180–188}$– and $gp100_{25–33}$–specific CD8$^+$ T cells was detected by pMHC multimer staining and flow cytometry.

Tumor growth was monitored at 3-day intervals using a digital caliper and tumor volume was calculated by the modified ellipsoidal formula: $V = (\text{length} \times \text{width}^2)/2$ (24). Mice were monitored daily for survival and were sacrificed when tumor length exceeded 20 mm.

Detection of naïve, effective, and memory CD8$^+$ T cells and regulatory T cells

SPCs were prepared, blocked by anti-mouse CD16/CD32, and then incubated with FITC-anti-mouse CD8, PE-anti-mouse CD44, and APC-anti-mouse CD62L for 30 minutes at 4°C. After washing with PBS, the cells were acquired on a FACSCalibur flow cytometer and analyzed with FlowJo software to identify CD44$^+$ cells and CD62L$^+$ cells in CD8$^+$ T-cell populations. For regulatory CD4$^+$ T cells, fresh SPCs were detected by using the mouse regulatory T-cell staining kit (eBiosciences). For regulatory CD8$^+$ T cells, fresh SPCs were blocked with anti-mouse CD16/CD32 first, and then stained with APC-anti-mouse CD3, FITC-anti-mouse CD8, and PE-anti-mouse CD28 for 30 minutes at 4°C. Finally, CD3$^+$/CD8$^+$/CD28$^-$ cells in CD8$^+$ T-cell populations were analyzed by flow cytometry.

Analyses of TRP2- and gp100-specific CTL degranulation

CD107a staining was performed as described (25), with modification. SPCs were incubated with $TRP2_{180–188}$ (or $gp100_{25–33}$) peptide (20 μg/mL) and PE-anti-CD107a for 1 hour at 37°C in a 5% CO_2 incubator, and followed by a 4-hour incubation in the presence of BFA/Monensin Mixture (MultiSciences). Then cells were stained with FITC-anti-mouse CD8 and the mixture of APC-anti-mouse IgG1 with H-2K^b/$TRP2_{180–188}$–Ig (or H-2D^b/$gp100_{25–33}$–Ig) for 1 hour at 4°C. Finally, the CD107a$^+$ cells in TRP2-Dimer$^+$/CD8$^+$ and gp100-Dimer$^+$/CD8$^+$ cell populations were analyzed by flow cytometry.

In vivo and *ex vivo* near-infrared imaging

To monitor the *in vivo* trafficking of MaAPCs, indocyanine green (ICG)-inlayed MaAPCs were prepared in the same way except that ICG (Sigma-Aldrich) was also dissolved in dichloromethane with PLGE polymer and other indicated molecules. Similarly, the ICG-inlayed Dimers$^-$MaAPCs (H-2K^b/$TRP2_{180–188}$–Ig dimers and H-2D^b/$gp100_{25–33}$–Ig dimers absent), CD47$^-$MaAPCs (CD47-Fc absent) and Blank-MPs were generated in parallel. On day 11 after melanoma cell challenge, the mice were randomized into four groups followed by injections of different ICG-MPs, respectively, via the tail vein (1×10^7 MPs/mouse). The mice were then anesthetized with Isoflurane and imaged by using Maestro *in vivo* fluorescence imaging system (Cri Inc.) at indicated time points. Images were captured at an excitation wavelength of 710–745 nm and an emission wavelength of 780–840 nm. At 2 hours after injection, mice were sacrificed; organs (liver, spleen, kidneys, lymph nodes, heart, and lungs) and tumor tissues were dissected for *ex vivo* imaging in the same conditions.

Colocalization of MaAPCs with immune cells *in vivo*

PE-labeled MaAPCs were generated by cocoupling PE–streptavidin (BD Biosciences) and other indicated molecules onto PEI-conjugated MP_{5+}. On day 11 after tumor cell challenge, PE-labeled control MPs and MaAPCs were injected, respectively, into the subcutaneous melanoma mice (1×10^7 MPs/mouse) via tail vein. Four hours later, spleens were collected in dark and embedded in freezing medium (OCT, Sakura Finetek Inc). Sections with a thickness of 5–7 μm were prepared. After being blocked with 10% mouse serum in PBS for 2 hours at 4°C, sections were incubated with FITC-anti-mouse CD19, FITC-anti-mouse CD4, FITC-anti-mouse CD8, FITC-anti-mouse DC11c, or FITC-anti-mouse F4/80 (eBiosciences) at 4°C overnight. After washing with PBS, sections were stained with DAPI (Sigma-Aldrich) for 5 minutes and finally visualized under confocal laser scanning microscopy (Olympus).

Published OnlineFirst May 21, 2019; DOI: 10.1158/2326-6066.CIR-18-0881

Statistical analyses

Statistical analyses were performed using GraphPad Prism 6.0 and SPSS Statistics 20.0 (IBM). All data are presented as the mean ± standard deviation (SD). The frequencies of antigen-specific T cells were compared across groups using ANOVA and Fisher LSD test. The release profile of immune molecules encapsulated in MaAPCs and tumor growth curves were analyzed by two-way repeated-measures ANOVA. To determine the mouse survival curve, a Kaplan–Meier graph was constructed, and a log-rank comparison of groups was used to calculate P values. *P* values of <0.05 were considered significant.

Results

Fabrication and characterization of PLGA-MP_{5+}

PLGA-MPs co-encapsulating IL2, IL15, CCL21, anti–CTLA-4 and anti–PD-1, termed MP_{5+}, were prepared, and conjugated with PEI for surface modification. MP_{5+} were spherical, with a smooth surface (Supplementary Fig. S1A), and mostly (82.5%) of diameters 3 to 7 μm with an average diameter of 4.5 ± 1.5 μm (Supplementary Fig. S1B). The mean ζ potential was 38.6 ± 5.1 mV, suggesting an ability to covalently couple proteins (Supplementary Fig. S1C).

The encapsulation efficiency of IL2, IL15, CCL21, anti–CTLA-4, and anti–PD-1 in the MP_{5+} was 81.5% to 83.0%, respectively, similar to the MP_{1+} which encapsulated only one kind of molecule (Supplementary Fig. S1D). All the encapsulated molecules can be released from the MP_{5+} in a sustained manner, with most (62.3%–71.0%) released during the first 2 days. The cumulative release efficiency of IL2, IL15, CCL21, anti–CTLA-4, and anti–PD-1 from MP_{5+} over 28 days was approximately 81.0% to 88.3%, respectively, similar to that from MP_{1+} (Supplementary Fig. S1E–S1I). Dynamic release curves of each indicated protein from MP_{5+} and MP_{1+} displayed no significant differences.

Generation and characterization of MaAPCs

MaAPCs (MP^{6+}_{5+}) were prepared (Supplementary Fig. S1J) and displayed shape and size similar to MP_{5+} (Supplementary Fig. S1K and S1L), but their ζ potential returned to neutral (Supplementary Fig. S1M). Flow cytometry revealed that each kind of surface molecules was coimmobilized successfully onto the surface of MaAPCs, with the fluorescence shift similar to the corresponding MP^{1+} in which only one kind of molecule was coupled, without encapsulation (Supplementary Fig. S1N). As shown in Supplementary Fig. S1O, each kind of soluble protein can be release from MaAPCs in a sustained manner, with release profiles similar to those of MP_{5+} (Supplementary Fig. S1E–S1I). The total amount of proteins encapsulated into 100 mg of PLGA polymer should be less than 60 mg. Otherwise, the PLGA-MPs cannot maintain the spherical shape and smooth surface (Supplementary Fig. S2A–S2C). In addition, the maximum absorption of protein on the surface of PLGA-MPs was 73 μg/5 × 10^6 MPs after PEI modification (Supplementary Fig. S2D–S2G).

In parallel, several control MPs were generated in a similar manner, such as MP^{2+}, MP^{5+}, MP^{6+}, MP^{6+}_{2+}, and MP^{6+}_{3+}, as described.

MaAPCs expand antigen-specific $CD8^+$ T cells *ex vivo* and enhance their cytotoxicity

Naïve SPCs from C57BL/6J mice were cocultured for 7 days with MaAPCs, MP^{6+}, MP_{5+}, or Blank-MPs. The frequencies of $TRP2_{180–188}$–specific $CD8^+$ T cells were expanded 268.4, 124.2, or 15.5 times by MaAPCs (51.0%), MP^{6+} (23.6%), or MP_{5+} (2.95%) stimulation as compared with Blank-MPs (0.19%). Similarly, $gp100_{25–33}$–specific $CD8^+$ T cells were expanded around 333.1, 166.9, or 16.6 times (Fig. 1A). Cytolysis of SPCs against B16 cells increased 814.3%, 559.2%, or 86.0% by MaAPCs, MP^{6+}, or MP_{5+} coculture relative to the Blank-MPs group at an E:T ratio of 50:1. SPCs from each group showed <10% to 20% of baseline cytolysis against non-cognate S180 cells and SP2/0 cells at various E:T ratios (Fig. 1B). The flow-cytometric histograms of 7-AAD staining for B16 cells were presented (Fig. 1C).

MaAPCs inhibit melanoma growth and augment antigen-specific CTL responses *in vivo*

To investigate the *in vivo* effects of MaAPCs on melanoma antigen–specific CTLs and tumor, C57BL/6J mice were injected s.c. with B16 cells or S180 cells on day 0, randomized into seven groups and infused i.v. with MaAPCs (MP^{6+}_{5+}), MP^{6+}_{3+}, MP^{6+}_{2+}, MP^{6+}, MP^{5+}, MP^{2+}, or Blank-MPs on days 7, 9, and 11 in an early therapeutic regimen (Fig. 1D). Tumor-bearing mice infused with MaAPCs showed reduction in melanoma growth relative to other MPs groups (Fig. 1E), and achieved the smallest tumor burden with a mean size of 172.8 mm^3 on day 28 (Fig. 1F). Moreover, the median survival times (MST) were 75, 65, 58, 49, 44, 37, and 32 days in the MaAPCs and control groups, respectively (Fig. 1G). Although growth of fibrosarcoma was inhibited by administration of MaAPCs, MP^{6+}_{3+}, MP^{6+}_{2+}, MP^{6+}, or MP^{5+}, inhibition of fibrosarcoma was less than that of melanoma (Fig. 1H and I). The statistical differences across groups were presented (Fig. 1J).

At the endpoint (day 28), the $TRP2_{180–188}$–specific and $gp100_{25–33}$–specific CTLs were detected in peripheral blood, spleens, and tumors in each group. In PBMCs (Fig. 2A), the percentages of $TRP2_{180–188}$–specific $CD8^+$ T cells were increased by 75, 63.1, 50.3, 21.6, 11.5, and 5.7-fold in MaAPCs, MP^{6+}_{3+}, MP^{6+}_{2+}, MP^{6+}, MP^{5+}, and MP^{2+} groups, respectively, as compared with Blank-MPs (0.16% ± 0.11%). Similar tendencies were also found for the frequencies of $gp100_{25–33}$–specific $CD8^+$ T cells. In SPCs (Fig. 2B), similar expansions of $TRP2_{180–188}$–specific and $gp100_{25–33}$–specific $CD8^+$ T were found in the indicated groups. In the single-cell suspensions derived from tumor tissues, the infiltrations of $TRP2_{180–188}$–specific $CD8^+$ T cells were also increased by 44.3-, 31.4-, 26.5-, 10.7-, 6.6-, or 2.8-fold whereas the $gp100_{25–33}$–specific $CD8^+$ T cells enhanced by 16.7-, 12.2-, 8.9-, 4.6-, 1.9-, or 1.2-fold in indicated groups (Fig. 2C). Histochemical staining confirmed that the MaAPC group displayed more necrotic tumor cells, apoptotic cells, and infiltrated $CD4^+$ or $CD8^+$ T cells in the melanoma tissues than Blank-MPs and PBS control groups (Fig. 2D).

MaAPCs facilitate activation of melanoma antigen–specific CTLs *in vivo*

In PBMCs (Fig. 3A; Supplementary Table S1), the frequencies of $TRP2_{180–188}$– and $gp100_{25–33}$–specific CTLs were enhanced 59.2 and 86.7 times, respectively, in the MaAPC group on day 14 as compared with the Blank-MPs group, and were also much higher than in the MP^{6+}_{3+}, MP^{6+}_{2+}, MP^{6+}, MP^{5+}, and MP^{2+} groups. Frequencies of $CD44^+$ cells in TRP2-Dimer$^+$ or gp100-Dimer$^+$ CTL populations were enhanced 56.0 or 63.7 times, whereas frequencies of $CD69^+$ cells were enhanced 9.0 or 9.5 times in MaAPCs group relative to the Blank-MP group. Similar tendencies

Published OnlineFirst May 21, 2019; DOI: 10.1158/2326-6066.CIR-18-0881

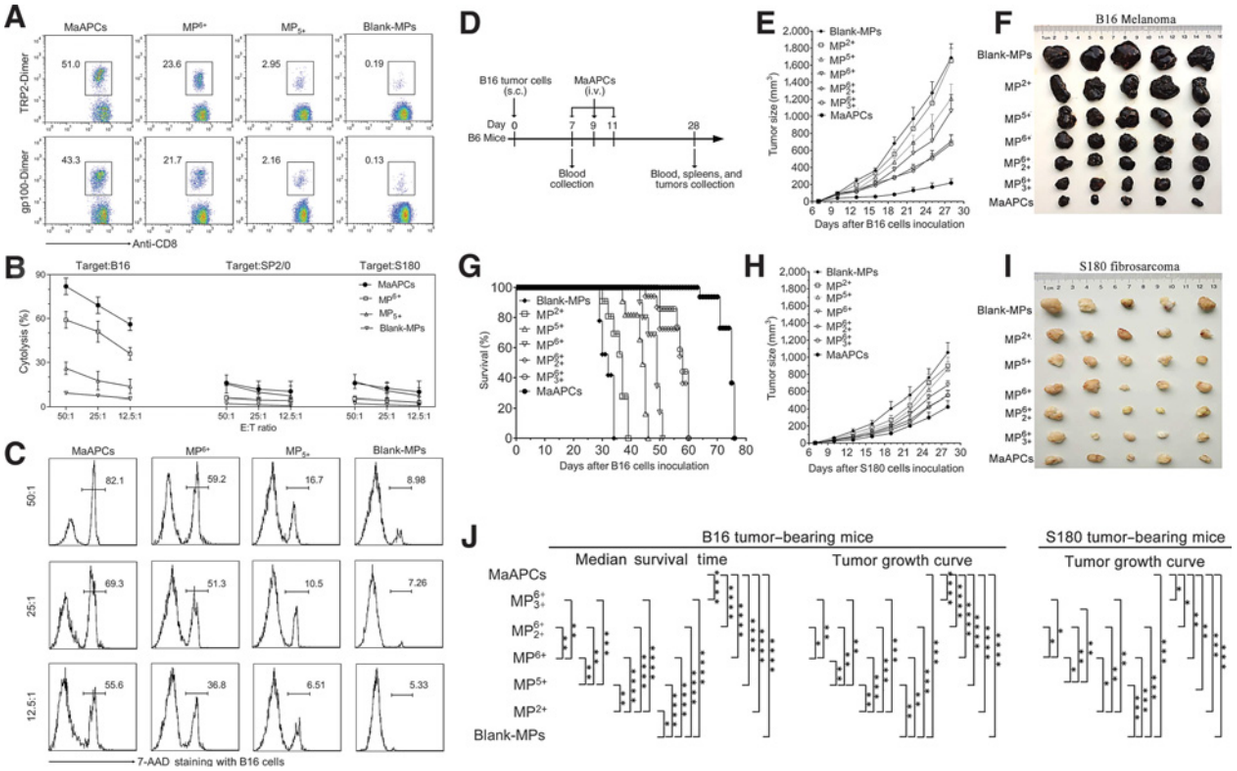

Figure 1.

MaAPCs enhance the expansion and cytotoxicity of melanoma antigen-specific CTLs *ex vivo* and inhibit melanoma growth in melanoma-bearing mice. Naïve splenocytes from C57BL/6J mice were coincubated for 7 days with MaAPCs, MP^{6+}, MP_{5+}, or Blank-MPs. MP^{6+}: the PLGA-MPs cocoupled with 6 kinds of surface molecules. **A,** The frequencies of $TRP2_{180–188}$–specific $CD8^+$ T cells and $gp100_{25–33}$–specific $CD8^+$ T cells in each coculture group, as detected by $TRP2_{180–188}$–dimer or $gp100_{25–33}$–dimer staining. Numbers in the top left of the dot plots represent the percentages of TRP2-$Dimer^+$ or gp100-$Dimer^+$ cells in the $CD8^+$ T-cell populations. **B,** Cytotoxicity of the splenocytes from the four indicated coculture groups. The resulting splenocytes were further cocultured with target cells for 4 hours at various E:T ratios followed by 7-AAD staining to analyze the cytolysis of B16, SP2/0, and S180 tumor cells. **C,** Representative flow-cytometric histograms of 7-AAD staining with B16 cells at various E:T ratios for the four coculture groups. These data were from one representative experiment of three independent experiments. **D,** Timeline for *in vivo* experiments. **E,** Subcutaneous melanoma growth ($n = 5$); **F**, melanoma tissues at endpoint (day 28, $n = 5$), and (**G**) Kaplan–Meier survival curves of melanoma-bearing mice ($n = 7$) in the treatment group of Blank-MPs, MP^{2+}, MP^{5+}, MP^{6+}, MP^{6+}_{2+}, MP^{6+}_{3+}, or MaAPCs (MP^{6+}_{5+}). **H,** Subcutaneous fibrosarcoma growth ($n = 5$) and (**I**) fibrosarcoma tissues at endpoint (day 28, $n = 5$) in the indicated groups. **J,** Statistical analyses for the differences across groups using a log-rank comparison for MST and two-way repeated-measures ANOVA for tumor growth curves. The presented data were from one representative experiment of two independent experiments. *, $P < 0.05$; **, $P < 0.01$; ***, $P < 0.001$; ****, $P < 0.0001$.

were also found in spleen lymphocytes (Fig. 3B; Supplementary Table S2) and the single-cell suspensions derived from tumor tissues (Fig. 3C; Supplementary Table S3). After MaAPC treatment, local infiltration of $TRP2_{180–188}$ and $gp100_{25–33}$–specific CTLs in tumor tissue was more on day 14 (205–212-fold expansion) than on day 28 (16–44-fold expansion). No differences in peripheral blood or spleen were evident between the two time points.

MaAPCs inhibit apoptosis and increase proliferation of melanoma antigen-specific CTLs

On day 14, SPCs were prepared from each treatment group and analyzed for apoptosis. The apoptotic cells in the TRP2-$Dimer^+$ CTL populations were reduced by 86.2%, 46.5%, 41.2%, and 34.1% in MaAPCs, MP^{6+}_{3+}, MP^{6+}_{2+}, and MP^{6+} groups, respectively, relative to the Blank-MP group (Fig. 4A). Similar tendencies were found for the apoptosis of gp100-$Dimer^+$ CTLs (Fig. 4B) and general $CD8^+$ T cells (Fig. 4C). The MP^{2+} treatment did not significantly reduce TRP2- and gp100-specific CTLs apoptosis. Statistical analyses across groups were presented in Fig. 4D.

To investigate the proliferation of TRP2- and gp100-specific CTLs in response to melanoma antigen *ex vivo*, SPCs from each group were prelabeled with CFSE and cocultured with $TRP2_{180–188}$ or $gp100_{25–33}$ peptides for 7 days. The proliferation rate of $TRP2_{180–188}$-specific $CD8^+$ T cells was 3.6, 2.8, 2.6, 2.0, 1.8, and 1.2 times, respetively, in MaAPCs, MP^{6+}_{3+}, MP^{6+}_{2+}, MP^{6+}, MP^{5+}, and MP^{2+} groups relative to the Blank-MP group (Fig. 4E). Similar tendencies were found for the proliferation of $gp100_{25–33}$–specific $CD8^+$ T cells (Fig. 4F) and general $CD8^+$ T cells (Fig. 4G). Statistical analyses across groups were presented in Fig. 4H.

MaAPCs elevate the cytotoxicity of melanoma antigen–specific CTLs *in vivo*

On day 14, SPCs were prepared from each group for the 4-hour cytolysis assay. As shown in Fig. 5A, the cytolysis of SPCs against B16 cells were enhanced 418.3%, 279.6%, 253.5%, 193.0%, 162.7%, and 36.6% at an E: T ratio of 50:1, respectively, in

Published OnlineFirst May 21, 2019; DOI: 10.1158/2326-6066.CIR-18-0881

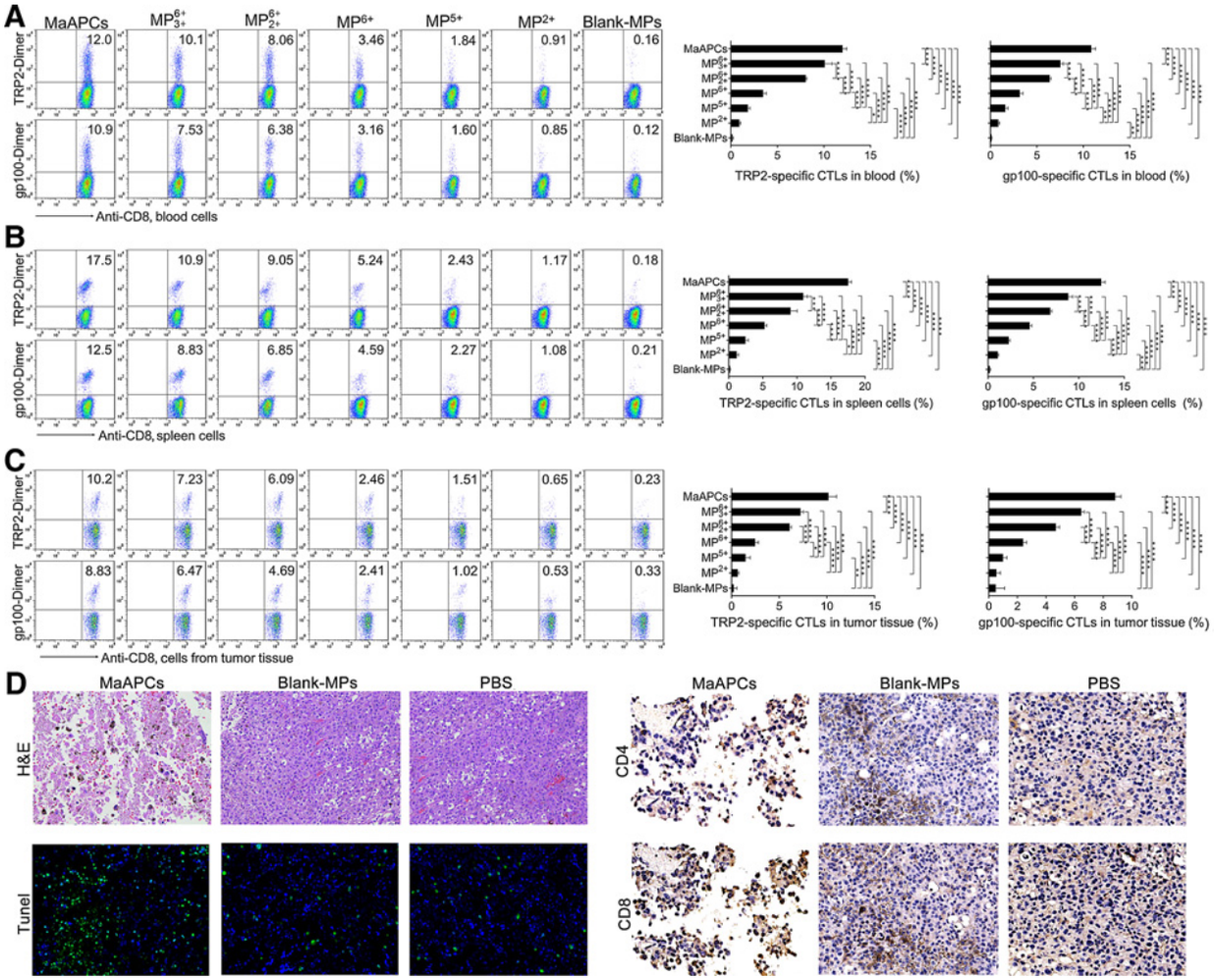

Figure 2.

MaAPCs augment melanoma antigen-specific CTL responses in melanoma-bearing mice. On day 28 (17 days after final infusion of MaAPCs or control MPs), the $TRP2_{180–188}$–specific and $gp100_{25–33}$–specific CTLs were detected in peripheral blood, spleens, and tumors for each treatment group, by TRP2-Dimer or gp100-Dimer staining and flow cytometry. The percentages of $TRP2_{180–188}$–specific CTLs and $gp100_{25–33}$–specific CTLs in the $CD8^+$ T-cell populations in PBMCs (**A**), spleen lymphocytes (**B**), and cell suspensions derived from melanoma tissues (**C**) were presented, along with the statistical analyses of differences across groups using ANOVA and Fisher LSD test ($n = 5$). Melanoma tissues were collected from MaAPCs, Blank-MPs and PBS treatment groups on day 28, sectioned, and followed with routine H&E staining, TUNEL fluorescence staining, and IHC staining with anti-mouse CD4 or anti-mouse CD8, respectively. Representative images from 3 mice per group were presented at 400× magnification (**D**). *, $P < 0.05$; **, $P < 0.01$; ***, $P < 0.001$; ****, $P < 0.0001$.

MaAPCs, MP^{6+}_{3+}, MP^{6+}_{2+}, MP^{6+}, MP^{5+}, and MP^{2+} groups when compared with the Blank-MPs group. Similar tendencies were found at the 25:1 or 12.5:1 ratio. SPCs from each group displayed less than 2% to 20% of baseline cytolysis against the non-cognate S180 cells and SP2/0 cells at various E:T ratios, but MaAPC treatment also significantly elevated the cytotoxicity of SPCs against SP2/O and S180 cells. MaAPC treatment significantly elevated the cytotoxicity of SPCs against SP2/0 and S180 cells. The 7-AAD staining with B16 cells (Fig. 5B), SP2/0 cells (Supplementary Fig. S3A), and S180 cells (Supplementary Fig. S3B) was presented.

To confirm the cytotoxicity of melanoma antigen-specific CTLs, CD107a on CTLs was assessed in the 5-hour cocultures of SPCs with TRP2 or gp100 peptides. The percentages of $CD107a^+$ cells in the TRP2-$Dimer^+$ CTL populations were 4.3, 3.1, 2.8, 1.7, 1.5, and 1.1 times, respectively, in MaAPCs, MP^{6+}_{3+}, MP^{6+}_{2+}, MP^{6+}, MP^{5+}, and MP^{2+} groups relative to the Blank-MP group (Fig. 5C). Similar tendencies were displayed in the gp100-$Dimer^+$ CTL populations (Fig. 5D) and general $CD8^+$ T-cell populations (Fig. 5E). The degranulation potential of CTLs was consistent with their cytolysis action against target cells. Statistical analyses for the percentages of $CD107a^+$ cells across groups were presented in Fig. 5F.

MaAPCs polarize memory $CD8^+$ T cells and reduce regulatory $CD4^+$ and $CD8^+$ T cells *in vivo*

On day 14, SPCs were collected from each group and assessed for memory $CD8^+$ T cells and Tregs. As shown in Fig. 6A and B, the frequencies of naïve $CD8^+$ T cells ($CD62L^+/CD44^{low}$) in MaAPC, MP^{6+}_{3+}, and MP^{6+}_{2+} groups reduced by 38.6%, 18.8%, and 14.1%, respectively, relative to the Blank-MP group (85.3% ± 8.49%).

Published OnlineFirst May 21, 2019; DOI: 10.1158/2326-6066.CIR-18-0881

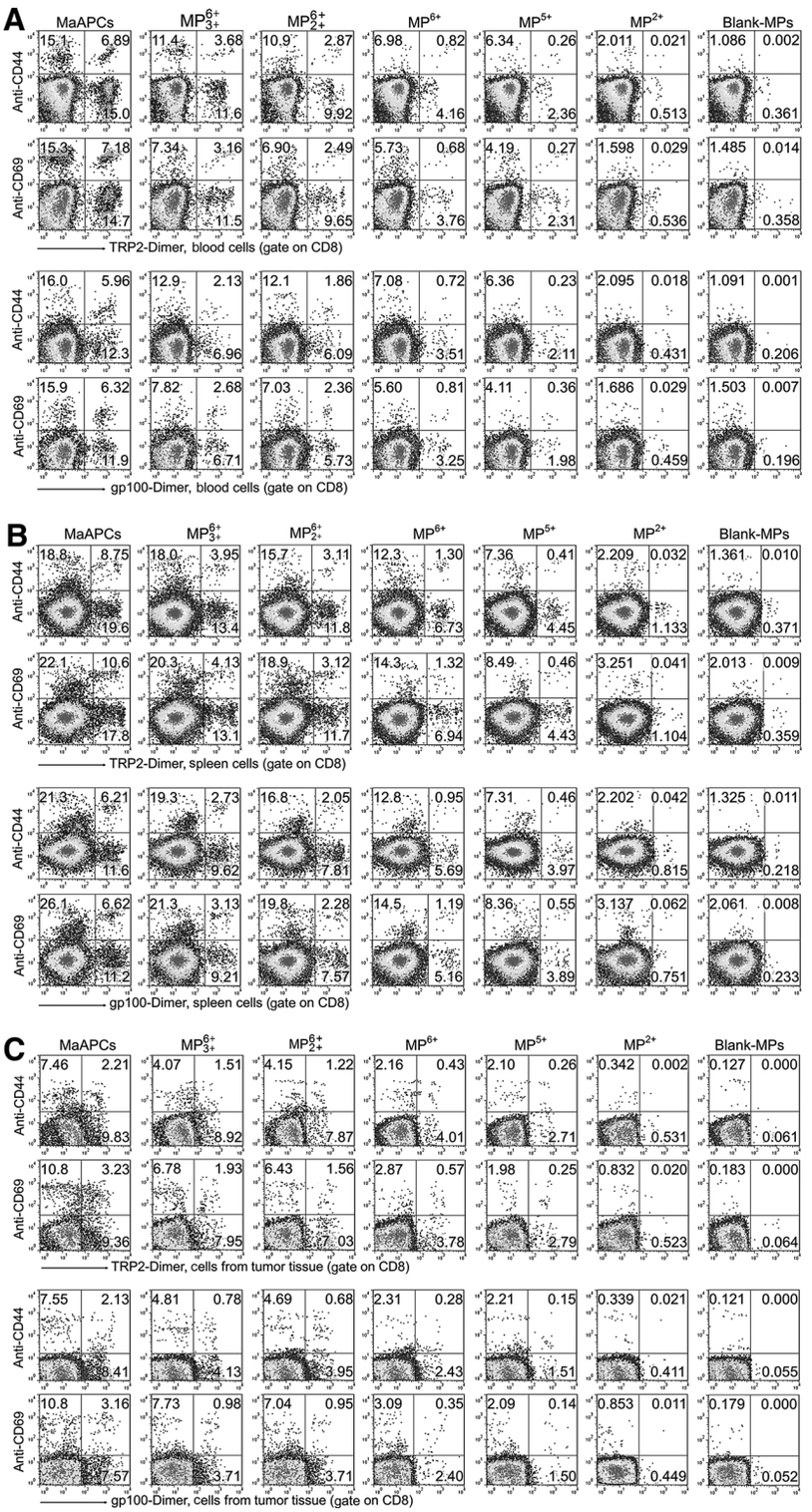

Figure 3.

MaAPCs facilitate activation of melanoma antigen-specific CTLs *in vivo*. PBMCs and SPCs were prepared from each melanoma-bearing mouse on day 14 (3 days after final infusion of MaAPCs or control MPs), and adjust to 1×10^7/mL. Melanoma tissues were isolated from each melanoma-bearing mouse and processed to the single-cell suspensions. Cells were blocked with anti-mouse CD16/CD32 first and stained later with the mixture of H-2K^b/TRP2$_{180-188}$–Ig dimer (or H-2D^b/gp100$_{25-33}$–Ig dimer) and APC-anti-mouse IgG1 for 1 hour at 4°C. Then FITC-anti-mouse CD8 and PE-anti-mouse CD44 (or PE-anti-mouse CD69) were added for another 30 minutes at 4°C, and followed by flow cytometry analyses. The frequencies of CD44$^+$ or CD69$^+$ cells in the TRP2-Dimer$^+$/CD8$^+$ T cell populations and in the gp100-Dimer$^+$/CD8$^+$ T cell populations from peripheral blood (**A**), spleen (**B**), and tumor tissue (**C**) were calculated, respectively. $n = 3$ or 4 mice per group.

Frequencies of activated and central memory CD8$^+$ T (CD62L$^+$/CD44$^{int\text{-}hi}$) in the three groups were 6.63, 3.84, and 3.77 times, respectively, relative to Blank-MPs (5.21% ± 0.80%), whereas the frequencies of effector memory CD8$^+$ T cells (CD62L$^-$/CD44^{hi}) were 5.99, 3.71, and 3.44 times, respectively, relative to Blank-MPs (1.12% ± 0.12%). MaAPC treatment reduced numbers of naïve CD8$^+$ T cells and expanded both central and effector memory CD8$^+$ T cells, but the treatments of MP^{6+}, MP^{5+}, or

Published OnlineFirst May 21, 2019; DOI: 10.1158/2326-6066.CIR-18-0881

MP^{2+} did not lead to the significant reduction of naïve $CD8^+$ T cells and expansion of central or effector memory $CD8^+$ T cells, implying the roles of the molecules co-encapsulated inside the MaAPCs in polarizing memory $CD8^+$ T cells.

In parallel, the frequencies of $CD4^+/CD25^+/Foxp3^+$ Tregs were reduced by 86.0%, 64.7%, 60.2%, and 47.6% in MaAPCs, MP^{6+}_{3+}, MP^{6+}_{2+}, and MP^{6+} groups, respectively, as compared with Blank-MPs, but no significant reduction was evident in the MP^{5+} and MP^{2+} groups (Fig. 6C). The frequencies of $CD8^+/CD28^-$ Tregs were decreased by 82.0%, 45.7%, 40.7%, and 27.3% in the indicated groups, respectively, but also no significant reduction was evident in the MP^{5+} and MP^{2+} groups (Fig. 6D). Percentages of effector $CD8^+$ T cells ($CD8^+/CD28^+$) were elevated by 178.4%, 99.4%, 88.6%, 59.4%, and 34.9% in MaAPCs, MP^{6+}_{3+}, MP^{6+}_{2+}, MP^{6+}, and MP^{5+} groups, respectively, although no significant increase was evident in the MP^{2+} group (Fig. 6D). Statistical differences across groups (Fig. 6E) were presented.

MaAPCs enhance IFNγ/TNFα production and decrease IL10/TGFβ secretion

On day 14, peripheral blood and spleens were harvested from each group and processed into plasma and SPCs. In fresh plasma, the concentrations of IFNγ/TNFα in MaAPCs, MP^{6+}_{3+}, MP^{6+}_{2+}, MP^{6+}, MP^{5+}, and MP^{2+} groups were 31.0/22.8 times, 21.7/14.5 times, 19.9/12.2 times, 12.7/6.01 times, 10.3/3.84 times, and 3.38/1.65 times higher, respectively, than in the Blank-MP group; However, the amount of IL10/TGFβ decreased by 78.0%/93.3%, 49.4%/64.2%, 46.9%/62.2%, 40.1%/43.4%, 35.2%/34.4%, and 4.29%/4.35% in the indicated treatment groups, respectively (Fig. 6F; Supplementary Table S4). In the culture supernatants of SPCs after 7-day incubation with $TRP2_{180–188}$ or $gp100_{25–33}$ peptides, similar tendencies of IFNγ/TNFα elevation and IL10/TGFβ reduction were also observed in the indicated treatment groups (Fig. 6G; Supplementary Table S5). MaAPCs treatment displayed the strongest functionality whereas MP^{2+} treatment exerted very weak impact on cytokine profiles.

In vivo trafficking and tissue distribution of MaAPCs in melanoma-bearing mice

To define the fate of MaAPCs *in vivo* and find out the roles of target antigens and "self-marker" CD47 molecules on MaAPCs, ICG-inlayed MaAPCs, $Dimer^-$ MaAPCs (TRP2-Dimer and gp100-Dimer absent), $CD47^-$ MaAPCs (CD47-Fc absent) or Blank-MPs were generated. Samples were injected via tail vein into mice with melanoma on day 11 after B16-cell challenge. *In vivo* and *ex vivo* near-infrared imaging followed. As revealed by whole-body fluorescence images at various time points (Fig. 7A), the fluorescence intensity in mice was strongest during the first 6 hours after ICG-MaAPCs injection, then decreased slowly, indicating a retention time of more than 36 hours. As controls, ICG-$Dimer^-$ MaAPCs, ICG-$CD47^-$ MaAPCs and ICG-Blank-MPs showed *in vivo* trafficking similar to that of ICG-MaAPCs, but with a shorter retention time and weaker fluorescent intensity from 6 to 36 hours (Fig. 7B). E*x vivo* imaging of dissected organs showed that at 2 hours after injection, MaAPCs and control MPs mainly appeared in liver, spleen, kidney, lungs, and lymph nodes with visible fluorescence (Fig. 7C). According to the mean fluorescence intensity, MaAPCs displayed significantly more accumulation in liver and lymph nodes, but less accumulation in kidney and lungs than the $CD47^-$MaAPCs, $Dimer^-$ MaAPCs, and Blank-MPs. $Dimer^-$ MaAPCs displayed more accumulation in liver and spleen, but less in kidney and lungs than $CD47^-$MaAPCs and Blank-MPs (Fig. 7D). No visible fluorescent signal of MaAPCs was observed in the tumor location over the 36 hours and in the excised tumor tissue at 2 hours, suggesting that most of the cell-sized MaAPCs could not go into the tumor through vascular circulation.

MaAPCs prefer to colocalize with $CD8^+$ T cells in melanoma-bearing mice

To ask whether MaAPCs can contact or interact with target CTLs *in vivo*, PE-labeled MaAPCs were generated and injected i.v. into melanoma-bearing mice on day 11 after B16 cells challenge. Four hours later, spleens were collected from each mouse. Frozen sections were prepared and followed by FITC-labeled mAb staining for $CD4^+$ T cells, $CD8^+$ T cells, B cells, macrophages, and dendritic cells. Confocal fluorescence images demonstrated that MaAPCs mainly distributed in the red pulp and marginal zone and presented many colocalizations with $CD8^+$ T cells, but fewer with other cells (Fig. 7E). These results indicate that MaAPCs contact $CD8^+$ T cells and are largely not engulfed by macrophage and dendritic cells *in vivo*.

MaAPCs treatment improves immune function without toxicity

The bystander effects of MaAPCs treatment were preliminarily investigated. Melanoma-bearing mice were randomized into three groups and administered via tail vein with PBS, Blank-MPs, or MaAPCs on days 7, 9, and 11 after B16 cells challenge. As compared with PBS and Blank-MP groups, MaAPC treatment did not significantly increase the frequencies of $CD4^+$ T cells, B cells, NK cells, macrophages, and DCs but led to a visible proliferation of $CD3^+$ T cells and $CD8^+$ T cells in the SPCs on day 14 (Supplementary Fig. S4A–S4G). Furthermore, routine blood tests were performed on days 14, 21, and 28 (3 days, 10 days, and 17 days after the final injection) in another independent experiment. White blood cell counts, lymphocyte counts, and percentages of lymphocytes displayed a visible elevation, whereas other cell populations showed no obvious bystander expansion at short time and longtime points after MaAPC treatment (Supplementary Fig. S4H).

Alloreactivity and antitumor effects are usually used as surrogate hallmarks for the retention of overall host immune function. On day 14, the SPCs were collected from each group and a third-party mixed lymphocyte reaction (MLR) assay followed. The alloreactive proliferation of T cells from the MaAPC group in response to the splenocytes from BALB/c mice showed significantly higher level than the T cells from the Blank-MPs and PBS groups (Supplementary Fig. S5A). The NK cells in SPC populations showed comparable cytolysis activity against Yac-1 lymphoma cells across the three groups (Supplementary Fig. S5B). In peripheral blood, the levels of melanoma cell–specific antibodies were not apparently different across the groups, but much higher than the naïve mice as detected by B16 cells incubation and FITC-anti-mouse IgG staining (Supplementary Fig. S5C). MaAPC treatment also significantly elevated the cytotoxicity of SPCs against non-cognate SP2/0 and S180 cells (Supplementary Fig. S3), and displayed significant inhibitory effects on S180 tumor growth, to some extent, as compared with Blank-MPs treatment (Fig. 1H–J). These data imply that MaAPCs treatment improved overall immune function of the

Published OnlineFirst May 21, 2019; DOI: 10.1158/2326-6066.CIR-18-0881

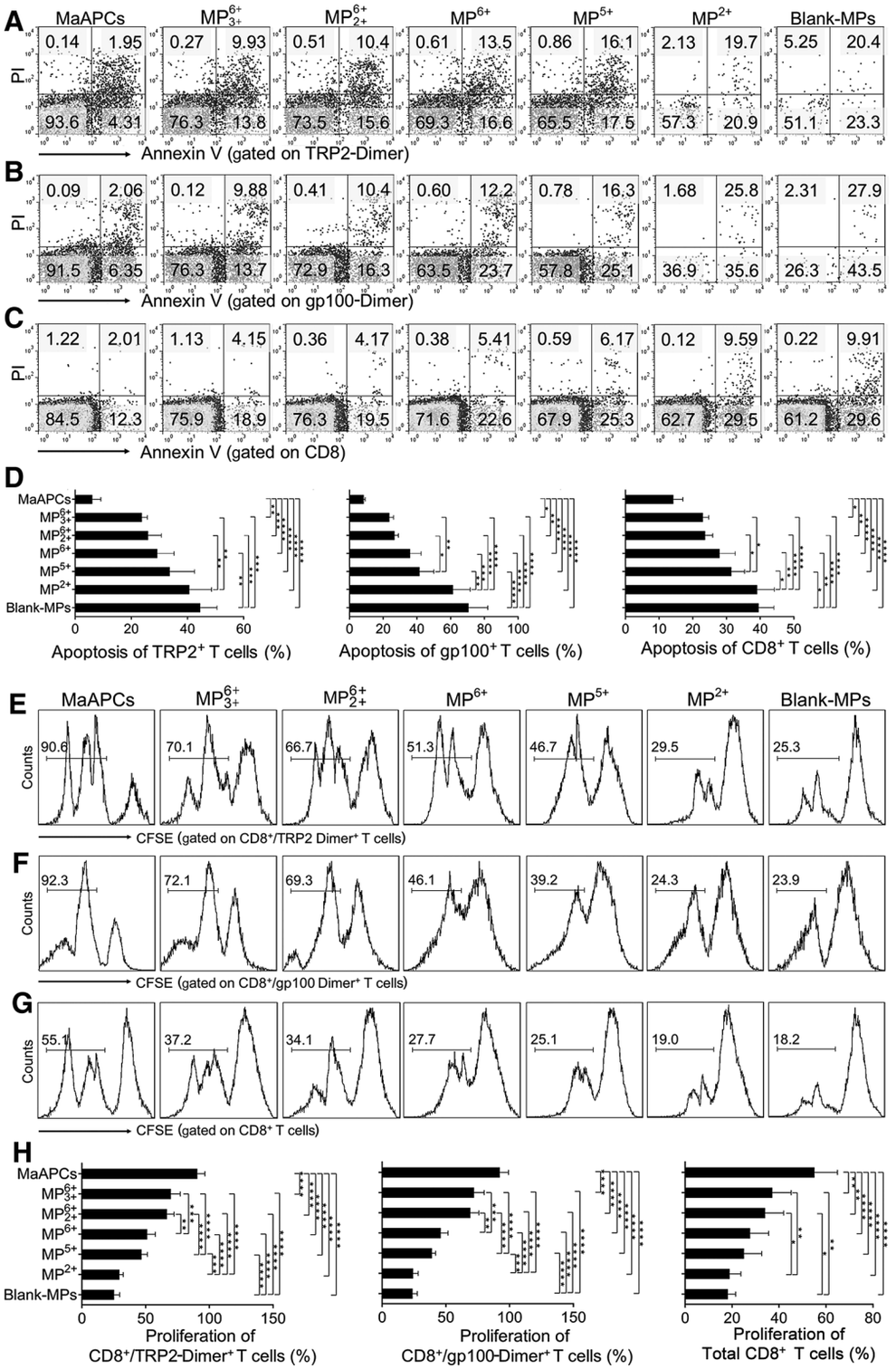

Figure 4.

MaAPCs inhibit apoptosis of melanoma antigen–specific CTLs and improve their proliferation *in vivo.* Spleen lymphocytes were isolated from melanoma-bearing mice at 3 days after final i.v. injection of MaAPCs or control MPs. After blocking with anti-mouse CD16/CD32, fresh SPCs were stained with the mixture of H-2K^b/TRP2-Ig (or H-2D^b/gp100-Ig) and APC-anti-mouseIgG1 for 1 hour at 4°C, then Annexin V and propidium iodide (PI) were added and incubated for 30 minutes at 4°C. To detect CD8$^+$ T-cell apoptosis, SPCs were stained with APC-anti-mouse CD8 first and Annexin V/PI later. Finally, the AnnexinV$^+$/PI$^+$ cells in H-2K^b/TRP2 Dimer$^+$, H-2D^b/gp100 Dimer$^+$, or CD8$^+$ cell populations were analyzed, respectively, by flow cytometry. (*Continued on the following page.*)

Published OnlineFirst May 21, 2019; DOI: 10.1158/2326-6066.CIR-18-0881

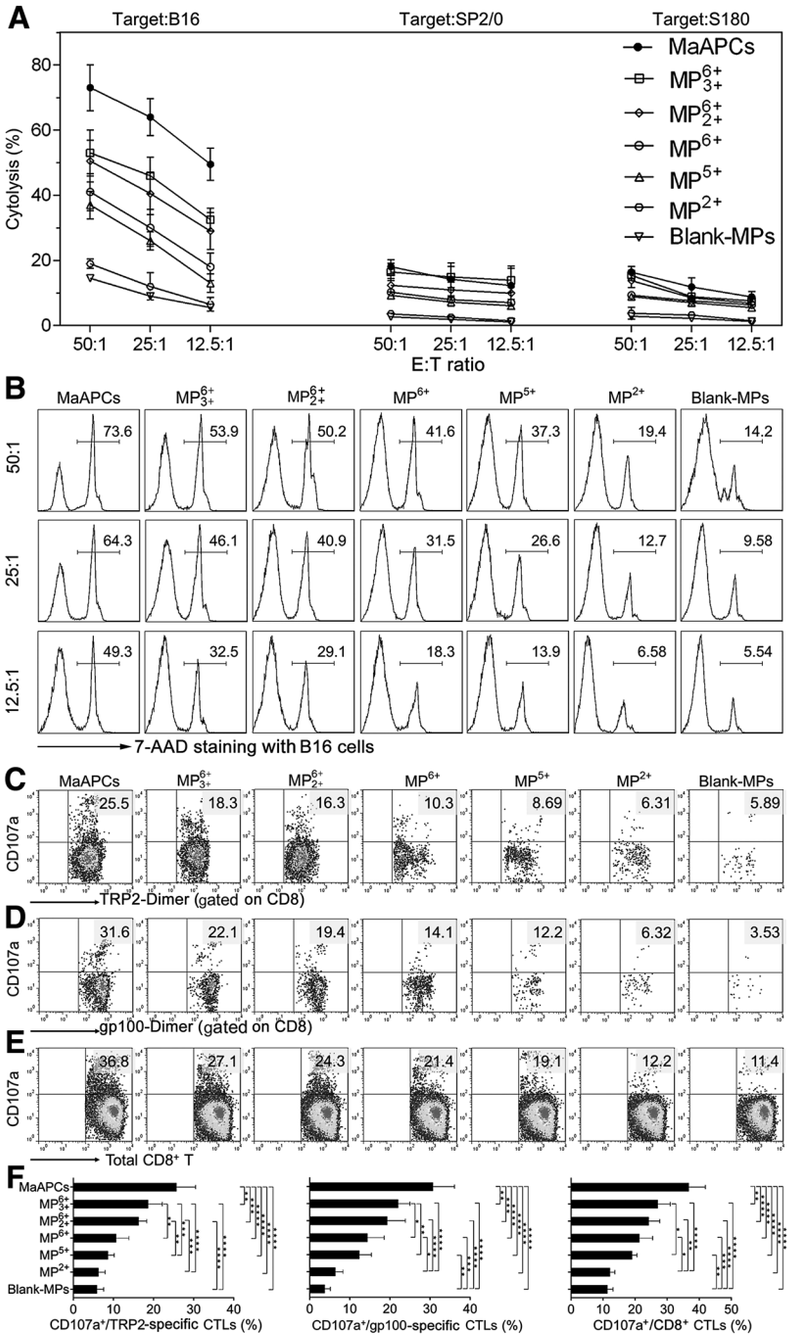

Figure 5.

MaAPCs elevate cytotoxicity of melanoma antigen-specific CTLs *in vivo*. Three days after the final infusion of MaAPCs or control MPs, spleen lymphocytes were prepared from each group and used as effector cells. The B16, S180, and SP2/0 cell lines were used, respectively, as target cells. Yac-1 cells were used to exhaust the NK cells presented in the spleen lymphocyte populations. After spleen lymphocytes and Yac-1 were prelabeled with CFSE, the 4-hour cytolysis assay was performed followed by 7-AAD staining. **A,** Cytotoxicity of spleen lymphocytes from each treatment group at various E:T ratios. **B,** Representative flow-cytometric histograms of 7-AAD staining with B16 cells for each treatment group. $n = 3$ or 4 mice per group. In parallel, spleen lymphocytes from each treatment group were cocultured with $TRP2_{180–188}$ or $gp100_{25–33}$ peptides for 5 hours, and followed by anti-CD107a, anti-CD8, and TRP2-Dimer or gp100-Dimer staining to monitor the degranulation of melanoma antigen-specific CTLs. **C,** Percentages of $CD107a^+$ cells in the TRP2-$Dimer^+$ CTL populations. **D,** Percentages of $CD107a^+$ cells in the gp100-$Dimer^+$ CTL populations. **E,** Percentages of $CD107a^+$ cells in the $CD8^+$ cell populations. **F,** Statistical analyses for the percentages of $CD107a^+$ cells across groups using ANOVA and Fisher LSD test. $n = 3$ or 4 mice per group. *, $P < 0.05$; **, $P < 0.01$; ***, $P < 0.001$; ****, $P < 0.0001$.

melanoma-bearing mice, to some extent, including the alloreactivity and ability inhibiting non-cognate tumors.

On days 14, 21, and 28, the functions of liver and kidney of melanoma-bearing mice were not impaired significantly by MaAPCs treatment as monitored by routine serum biochemical tests of peripheral blood (Supplementary Fig. S5D). No visible damage was observed in the tissue sections of spleen, kidney, liver, heart, and lungs after MaAPCs treatment when

(*Continued.*) **A,** Frequencies of apoptotic TRP2-$Dimer^+$ T cells. **B,** Frequencies of apoptotic gp100-$Dimer^+$ T cells. **C,** Frequencies of apoptotic $CD8^+$ T cells. **D,** Statistical analyses for percentages of apoptotic cells across groups using ANOVA and Fisher LSD test. In addition, SPCs were prelableld with CFSE, then seeded into round-bottom 96-well plates (1×10^6 cells/well) and coincubated with $TRP2_{180–188}$ or $gp100_{25–33}$ peptides (20 μg/mL) for 7 days in complete RPMI-1640 medium containing 10% FBS and IL2 (100 IU/mL). Cells were harvested, stained with the mixture of APC-anti-mouse IgG1, and H-$2K^b$/$TRP2_{180–188}$–Ig (or H-$2D^b$/$gp100_{5–33}$–Ig) for 30 minutes at 4°C, then PE-anti-mouse CD8 was added for another 30 minutes at 4°C. Finally, the proliferation of $CD8^+$/$Dimer^+$ T cells was analyzed according to the reduction of CFSE-staining brightness. **E,** Proliferation percentages of $CD8^+$/TRP2-$Dimer^+$ T cells. **F,** Proliferation percentages of $CD8^+$/gp100-$Dimer^+$ T cells. **G,** Proliferation percentages of $CD8^+$ T cells. **H,** Statistical analyses for proliferation percentages across groups using ANOVA and Fisher LSD test. $n = 3$ or 4 mice per group. *, $P < 0.05$; **, $P < 0.01$; ***, $P < 0.001$; ****, $P < 0.0001$.

Published OnlineFirst May 21, 2019; DOI: 10.1158/2326-6066.CIR-18-0881

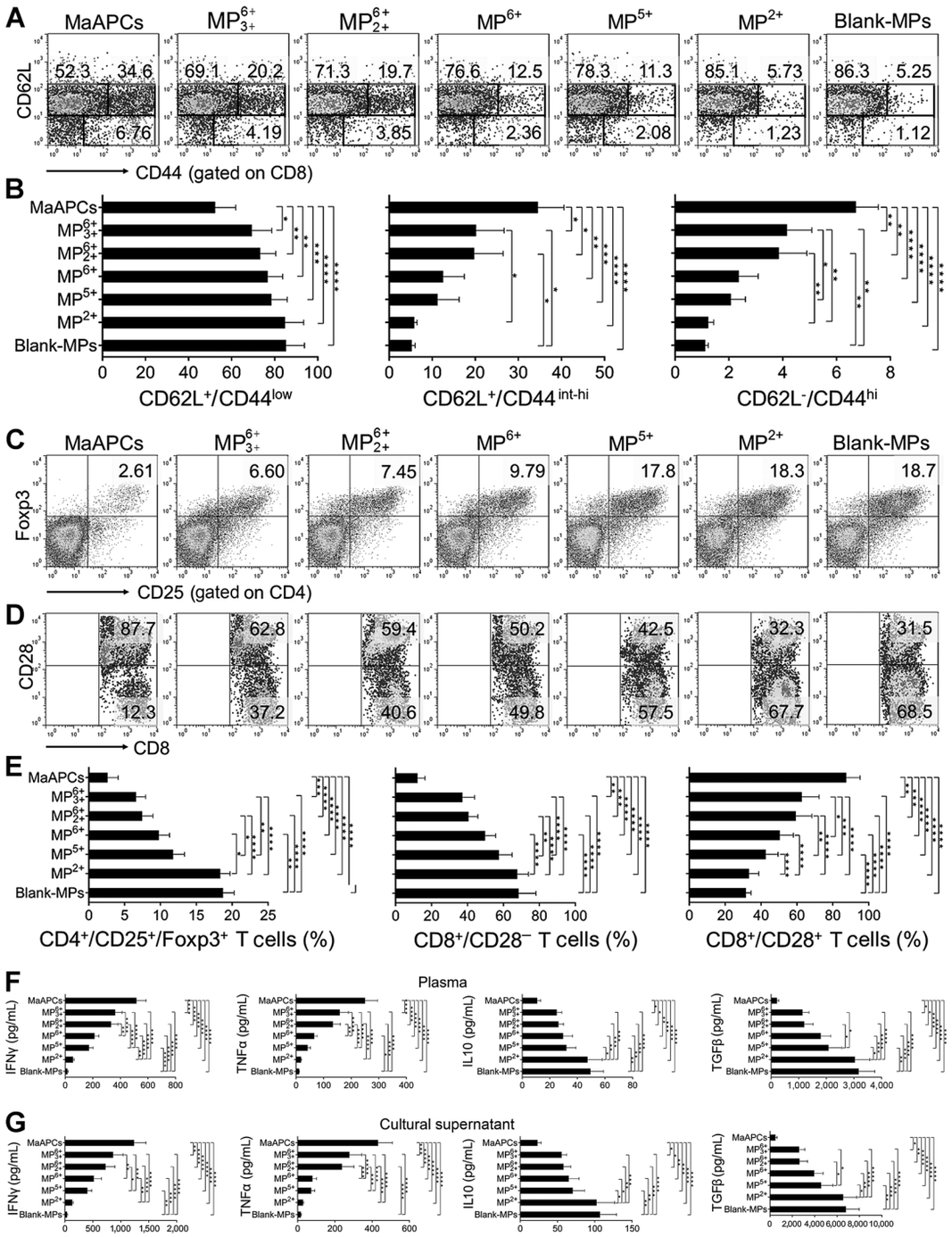

Figure 6.

MaAPCs polarize memory CD8$^+$ T cells, reduce regulatory CD4$^+$ and CD8$^+$ T cells, enhance IFNγ/TNFα production, and decrease IL10/TGFβ secretion *in vivo*. Three days after the final infusion of MaAPCs or control MPs, the peripheral blood and spleens were collected from each tumor-bearing mouse and processed into plasma and spleen lymphocytes. **A,** Three-color fluorescence staining of CD8/CD62L/CD44 for the fresh spleen lymphocytes from each treatment group. **B,** Statistical analyses for the percentages of memory CD8$^+$ T cells across groups. **C,** Three-color staining of CD4/CD25/Foxp3 for the fresh spleen lymphocytes from each treatment group. **D,** Two-color staining of CD8/CD28 for the fresh spleen lymphocytes from each treatment group. **E,** Statistical analyses for the percentages of regulatory CD4$^+$ and CD8$^+$ T cells across groups. In addition, spleen lymphocytes were prelabeled with CFSE and coincubated with $TRP2_{180–188}$ or $gp100_{25–33}$ peptides (20 μg/mL) in round-bottom 96-well plates (1×10^6 cells/well) for 7 days in complete RPMI-1640 medium containing 10% FBS and 100 IU/mL IL2. Concentrations of cytokines IFNγ, TNFα, IL10, and TGFβ in the fresh plasma (**F**) and in the culture supernatants of spleen lymphocytes (**G**) were quantified by ELISA kits (Dakewe Biotech). $n = 3$ or 4 mice per group in each independent experiment. Differences across groups were analyzed using ANOVA and Fisher LSD test. *, $P < 0.05$; **, $P < 0.01$; ***, $P < 0.001$; ****, $P < 0.0001$.

Published OnlineFirst May 21, 2019; DOI: 10.1158/2326-6066.CIR-18-0881

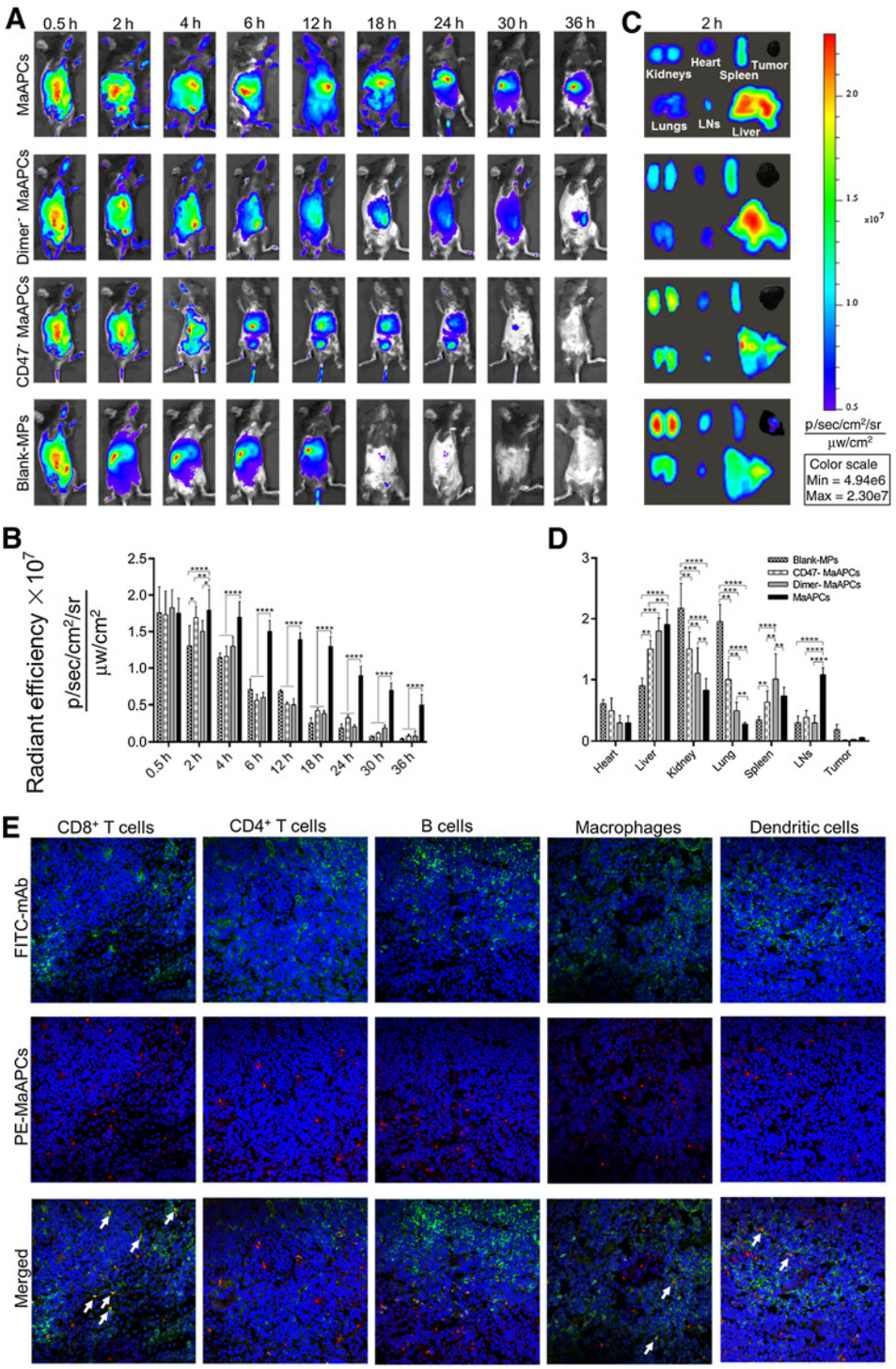

Figure 7.

In vivo trafficking of MaAPCs in melanoma-bearing mice and colocalizations with immune cells. ICG-inlayed MaAPCs, Dimer$^-$ MaAPCs (TRP2-Dimer and gp100-Dimer absent), CD47$^-$ MaAPCs (CD47-Fc absent), or Blank-MPs were generated, injected i.v. into the melanoma mice on day 11 after B16 cells challenge, and followed by *in vivo* and *ex vivo* near-infrared imaging. **A,** Whole-body near-infrared imaging at indicated time points after i.v. injection of ICG-inlayed MaAPCs or control MPs. **B,** The mean intensities of fluorescence in whole body at indicated time points. **C,** *Ex vivo* near-infrared imaging for organs dissected surgically from melanoma mice at 2-hour time point after i.v. injection of ICG-inlayed MaAPCs or control MPs. **D,** The mean intensities of fluorescence in dissected organs. $n = 3$ mice/time point/group. Differences across groups were analyzed using ANOVA and Fisher LSD test. *, $P < 0.05$; **, $P < 0.01$; ***, $P < 0.001$; ****, $P < 0.0001$. **E,** Spleens were collected from melanoma-bearing mice at 4 hours after i.v. injection of PE-labeled MaAPCs. Frozen sections were prepared. Then, CD8$^+$ T cells, CD4$^+$ T cells, B cells, macrophages, and DCs were stained with FITC-labeled mAbs, respectively, and observed by confocal imaging. Representative images from 3 mice were presented at 400× magnification. White arrow points at the colocalizations of MaAPCs with stained cells.

compared with the Blank-MPs or PBS treatments, as analyzed by H&E staining at the same time points (Supplementary Fig. S6A–S6E). Both functional and histopathological analyses suggest that the MaAPCs treatment did not cause apparent organ toxicity at the longtime points in the subcutaneous melanoma mice.

Discussion

PLGA micro- or nanoparticles (PLGA-MNPs) have been used as scaffolds to generate biodegradable and polymeric aAPCs by cocoupling pMHC molecules and anti-CD28 onto the spherical or ellipsoidal PLGA-MNPs. Some studies have used IL2 encapsulated inside as a third signal. These studies have used PLGA-MNPs

Published OnlineFirst May 21, 2019; DOI: 10.1158/2326-6066.CIR-18-0881

to expand antigen-specific T cells *in vitro* (26–28) or in mice models (29–31). Previously, we developed a four-signal aAPCs system by cocoupling H-2K^b/TRP2-Ig dimer and anti-CD28 onto PLGA-MPs with IL2 and anti–CTLA-4 encapsulated inside (22).

Here, we used up to 11 kinds of immune molecules co-carried by the cell-sized PLGA-MPs to simulate natural APCs. Both *in vitro* and *in vivo* data displayed the feasibility of bispecific aAPCs delivering H-2K^b/TRP2$_{180–188}$–Ig and H-2K^b/gp100$_{25–33}$–Ig dimers as target antigens, but the MP^{2+} exerted weak effects on T cells, similar to Blank-MPs, indicating the failure of target antigens alone to elicit T-cell responses. MP^{5+} induced anti-melanoma responses *in vivo*, such as enhancing the activation, proliferation, cytotoxicity of TRP2- and gp100-specific CTLs, and their infiltration in tumor tissue, as well as reducing IL10 and TGFβ, elevating IFNγ but not TNFα. These results defined the stimulatory functionality of costimulatory molecules (anti-CD28, anti-4-1BB, and anti-CD2) onto MaAPCs, although we had not clarified the contributions *in vivo* of each molecule and their synergistic effects. Unlike previous reports (32–34), the target antigens and costimulatory molecules on MaAPCs did not polarize central and effector memory T cells or inhibit regulatory T cells. As compared with the MP^{5+}, the MP^{6+} (MP^{5+} cocoupled with CD47-Fc) initiated more rigorous anti-melanoma immune response, including more effectively activating and expanding antigen-specific CTLs, improving their cytotoxicity, inhibiting their apoptosis, and regulatory T cell production. Moreover, the CD47$^+$ MaAPCs displayed more accumulation in lymphoid tissues and a longer retention time relative to the CD47$^-$ MaAPCs. These data suggest that the CD47 molecule, a "self-marker" used to construct the "stealth particles" in NP-mediated drug delivery systems in human (35, 36), can enhance the therapeutic effects of MaAPCs, perhaps by minimizing phagocytosis.

Here, we co-encapsulated cytokines (IL2, IL15), chemokine (CCL21), and checkpoint inhibitors (anti–CTLA-4, anti–PD-1) inside MaAPCs. To evaluate their individual contributions *in vivo*, several control groups were also analyzed. MP$^{6+}_{2+}$ (MP^{6+} encapIL2/IL15) elicited stronger immune responses than MP^{6+}, with differences in various immune parameters. Furthermore, MP$^{6+}_{5+}$ (MaAPCs) induced more rigorous immune responses than MP$^{6+}_{2+}$. These differences confirmed the role of IL2/IL15 and contributions of anti–CTLA-4/anti–PD-1 in the therapeutic effects. We did not further distinguish between the contributions of IL2 and IL15 or anti–CTLA-4 and anti–PD-1 due to the requirement of too many control groups. No differences were found between MP$^{6+}_{2+}$ and MP$^{6+}_{3+}$ (MP^{6+} encap IL2/IL15/CCL21) groups on various immune parameters, including the infiltration of CTLs in tumor. The weak effects of CCL21 may be attributed to the intravenous injection of MaAPCs. After infusion by tail vein, the cell-sized MaAPCs circulated into various organs and secondary lymphoid tissues, but few into tumor tissue. MaAPCs exerted direct effects on antigen-specific T cells mainly in spleen and lymph nodes where plenty of T cells homing without the requirement for chemokines. Therefore, the infiltration of antigen-specific CTLs into melanoma tissue may not be due to the release of CCL21 from MaAPCs.

In this study, the five kinds of proteins, representing a range of molecule weights, had no obvious influence on each other when co-encapsulated inside the PLGA-MPs and co-released from the MPs. The six kinds of surface molecules had no obvious influence on each other when cocoupled onto MaAPCs, and the cocoupling of multiple surface molecules did not impair the sustained co-release of molecules from the MaAPCs. To achieve these results, we optimized the amount and ratio of each molecule according to its function and molecular weight. We found that intraperitoneal (i.p.), subcutaneous (s.c.), and tumor local injections cannot be used because they only caused weak immune responses and limited clinical effect. Perhaps acellular aAPCs cannot freely move *in vivo* after i.p, s.c., or local injections, thus resulting in few contacts with T cells if injected into less than ideal locations.

In conclusion, an 11-signal MaAPC was developed and exerted stronger effects on T cells by surface presentation and paracrine release than the control aAPCs carrying 9, 8, 6, 5, or 2 kinds of indicated immune molecules. Such cell-free aAPCs may present an avenue for treatment of tumors as patient-individualized (HLA-restricted) and antigen-specific immunotherapy.

Disclosure of Potential Conflicts of Interest

No potential conflicts of interest were disclosed.

Authors' Contributions

Conception and design: C. Shen
Development of methodology: L. Zhang, S. Song, X. Jin , X. Wan, K.A. Shahzad, W. Pei, C. Zhao
Acquisition of data (provided animals, acquired and managed patients, provided facilities, etc.): L. Zhang, S. Song, X. Jin, X. Wan, W. Pei, and C. Zhao
Analysis and interpretation of data (e.g., statistical analysis, biostatistics, computational analysis): L. Zhang, C. Shen, S. Song, X. Jin, X. Wan
Writing, review, and/or revision of the manuscript: L. Zhang, K.A. Shahzad, C. Shen
Administrative, technical, or material support (i.e., reporting or organizing data, constructing databases): L. Zhang, C. Shen, W. Pei, C. Zhao
Study supervision: L. Zhang, C. Shen

Acknowledgments

This work was supported by grants from the National Natural Science Foundation of China (81372448) and the Science and Technology Support Program of Jiangsu Province (BE2017714) for C. Shen. The sponsors had no role in study design, data collection and analysis, preparation of the manuscript, or decision to submit the article for publication.

The costs of publication of this article were defrayed in part by the payment of page charges. This article must therefore be hereby marked *advertisement* in accordance with 18 U.S.C. Section 1734 solely to indicate this fact.

Received December 10, 2018; revised February 19, 2019; accepted May 17, 2019; published first May 21, 2019.

References

1. Hu Z, Xia J, Fan W, Wargo J, Yang YG. Human melanoma immunotherapy using tumor antigen-specific T cells generated in humanized mice. Oncotarget 2016;7:6448–59.
2. Osada T, Nagaoka K, Takahara M, Yang XY, Liu CX, Guo H, et al. Precision cancer immunotherapy: optimizing dendritic cell-based strategies to induce tumor antigen-specific T-cell responses against individual patient tumors. J Immunother 2015;38: 155–64.
3. Zhang N, Bevan MJ. CD8(+) T cells: foot soldiers of the immune system. Immunity 2011;35:161–8.
4. Bhargava A, Mishra D, Banerjee S, Mishra PK. Dendritic cell engineering for tumor immunotherapy: from biology to clinical translation. Immunotherapy 2012;4:703–18.
5. Bol KF, Schreibelt G, Gerritsen WR, de Vries IJ, Figdor CG. Dendritic cell-based immunotherapy: state of the art and beyond. Cancer Res 2016;22: 1897–906.

6. Kim JV, Latouche JB, Riviere I, Sadelain M. The ABCs of artificial antigen presentation. Nat Biotechnol 2004;22:403–10.
7. Butler MO, Hirano N. Human cell-based artificial antigen-presenting cells for cancer immunotherapy. Clin Cancer Res 2014;257:191–209.
8. Eggermont LJ, Paulis LE, Tel J, Figdor CG. Towards efficient cancer immunotherapy: advances in developing artificial antigen-presenting cells. Trends Biotechnol 2014;32:456–65.
9. Goto T, Nishida T, Takagi E, Miyao K, Koyama D, Sakemura R, et al. Programmed death-ligand 1 on antigen-presenting cells facilitates the induction of antigen-specific cytotoxic T lymphocytes: application to adoptive T-cell immunotherapy. J Immunother 2016;39:306–15.
10. Sun L, Guo H, Jiang R, Lu L, Liu T, Zhang Z, et al. Artificial antigen-presenting cells expressing AFP(158-166) peptide and interleukin-15 activate AFP-specific cytotoxic T lymphocytes. Oncotarget 2016;7: 17579–90.
11. Garnier A, Hamieh M, Drouet A, Leprince J, Vivien D, Frebourg T, et al. Artificial antigen-presenting cells expressing HLA class II molecules as an effective tool for amplifying human specific memory CD4(+) T cells. Immunol Cell Biol 2016;94:662–72.
12. Perica K, Kosmides AK, Schneck JP. Linking form to function: biophysical aspects of artificial antigen presenting cell design. Biochim Biophys Acta 2015;1853:781–90.
13. Bruns H, Bessell C, Varela JC, Haupt C, Fang J, Pasemann S, et al. CD47 enhances in vivo functionality of artificial antigen-presenting cells. Clin Cancer Res 2015;21:2075–83.
14. Perica K, Bieler JG, Schutz C, Varela JC, Douglass J, Skora A, et al. Enrichment and expansion with nanoscale artificial antigen presenting cells for adoptive immunotherapy. ACS Nano 2015;9:6861–71.
15. Durai M, Krueger C, Ye Z, Cheng L, Mackensen A, Oelke M, et al. In vivo functional efficacy of tumor-specific T cells expanded using HLA-Ig based artificial antigen presenting cells (aAPC). Cancer Immunol Immunother 2009;58:209–20.
16. Lu XL, Jiang XB, Liu RE, Zhang SM, Liang ZH. In vivo anti-melanoma efficacy of allo-restricted CTLs specific for melanoma expanded by artificial antigen-presenting cells. Cancer Immunol Immunother 2009;58:629–38.
17. Chiu YL, Schneck JP, Oelke M. HLA-Ig based artificial antigen presenting cells for efficient ex vivo expansion of human CTL. J Vis Exp 2011. pii: 2801.
18. Shen C, Cheng K, Miao S, Wang W, He Y, Meng F, et al. Latex bead-based artificial antigen-presenting cells induce tumor-specific CTL responses in the native T-cell repertoires and inhibit tumor growth. Immunol Lett 2013; 150:1–11.
19. Pagels RF, Prud'homme RK. Polymeric nanoparticles and microparticles for the delivery of peptides, biologics, and soluble therapeutics. J Control Release 2015;219:519–35.
20. Kapoor DN, Bhatia A, Kaur R, Sharma R, Kaur G, Dhawan S. PLGA: a unique polymer for drug delivery. Ther Deliv 2015;6:41–58.
21. Han FY, Thurecht KJ, Whittaker AK, Smith MT. Bioerodable PLGA-based microparticles for producing sustained-release drug formulations and strategies for improving drug loading. Front Pharmacol 2016;7:185.
22. Zhang L, Wang L, Shahzad KA, Xu T, Wan X, Pei W, et al. Paracrine release of IL2 and anti-CTLA-4 enhances the ability of artificial polymer antigen-presenting cells to expand antigen-specific T cells and inhibit tumor growth in a mouse model. Cancer Immunol Immunother 2017;66:1229–41.
23. Donat U, Rother J, Schafer S, Hess M, Hartl B, Kober C, et al. Characterization of metastasis formation and virotherapy in the human C33A cervical cancer model. PLoS One 2014;9:e98533.
24. Geekiyanage H, Galanis E. MiR-31 and miR-128 regulates poliovirus receptor-related 4 mediated measles virus infectivity in tumors. Mol Oncol 2016;10:1387–403.
25. Betts MR, Brenchley JM, Price DA, De Rosa SC, Douek DC, Roederer M, et al. Sensitive and viable identification of antigen-specific CD8+ T cells by a flow cytometric assay for degranulation. J Immunol Methods 2003;281: 65–78.
26. Steenblock ER, Fadel T, Labowsky M, Pober JS, Fahmy TM. An artificial antigen-presenting cell with paracrine delivery of IL-2 impacts the magnitude and direction of the T cell response. J Biol Chem 2011;286: 34883–92.
27. Han H, Peng JR, Chen PC, Gong L, Qiao SS, Wang WZ, et al. A novel system of artificial antigen-presenting cells efficiently stimulates Flu peptide-specific cytotoxic T cells in vitro. Biochem Biophys Res Commun 2011; 411:530–5.
28. Steenblock ER, Fahmy TM. A comprehensive platform for ex vivo T-cell expansion based on biodegradable polymeric artificial antigen-presenting cells. Mol Ther 2008;16:765–72.
29. Sunshine JC, Perica K, Schneck JP, Green JJ. Particle shape dependence of CD8+ T cell activation by artificial antigen presenting cells. Biomaterials 2014;35:269–77.
30. Meyer RA, Sunshine JC, Perica K, Kosmides AK, Aje K, Schneck JP, et al. Biodegradable nanoellipsoidal artificial antigen presenting cells for antigen specific T-cell activation. Small 2015;11:1519–25.
31. Kosmides AK, Meyer RA, Hickey JW, Aje K, Cheung KN, Green JJ, et al. Biomimetic biodegradable artificial antigen presenting cells synergize with PD-1 blockade to treat melanoma. Biomaterials 2017;118:16–26.
32. Rudolf D, Silberzahn T, Walter S, Maurer D, Engelhard J, Wernet D, et al. Potent costimulation of human CD8 T cells by anti-4-1BB and anti-CD28 on synthetic artificial antigen presenting cells. Cancer Immunol Immunother 2008;57:175–83.
33. Ye Q, Loisiou M, Levine BL, Suhoski MM, Riley JL, June CH, et al. Engineered artificial antigen presenting cells facilitate direct and efficient expansion of tumor infiltrating lymphocytes. J Transl Med 2011;9:131.
34. Yang JJ, Ye Y, Carroll A, Yang W, Lee HW. Structural biology of the cell adhesion protein CD2: alternatively folded states and structure-function relation. Curr Protein Pept Sci 2001;2:1–17.
35. Tsai RK, Rodriguez PL, Discher DE. Self inhibition of phagocytosis: the affinity of `marker of self' CD47 for SIRPalpha dictates potency of inhibition but only at low expression levels. Blood Cells Mol Dis 2010;45: 67–74.
36. Massarelli E, Papadimitrakopoulou V, Welsh J, Tang C, Tsao AS. Immunotherapy in lung cancer. Transl Lung Cancer Res 2014;3:53–63.

Published OnlineFirst May 21, 2019; DOI: 10.1158/2326-6066.CIR-18-0881

Cancer Immunology Research

An Artificial Antigen-Presenting Cell Delivering 11 Immune Molecules Expands Tumor Antigen–Specific CTLs in *Ex Vivo* and *In Vivo* Murine Melanoma Models

Lei Zhang, Shilong Song, Xiaoxiao Jin, et al.

Cancer Immunol Res 2019;7:1188-1201. Published OnlineFirst May 21, 2019.